Allelochemicals of Alexandrium minutum: Kinetics of membrane disruption and photosynthesis inhibition in a co-occurring diatom

Marc Long, Alexandra Peltekis, Carmen González-Fernández, Helene Hegaret, Benjamin Bailleul

Allelochemicals of *Alexandrium minutum*: kinetics of membrane disruption and photosynthesis inhibition in a co-occurring diatom

Marc Long[1,2*], Alexandra Peltekis[3*], Carmen González-Fernández[4], Hélène Hégaret[2], Benjamin Bailleul[3]

[1] School of Chemistry, University of Wollongong, NSW 2522, Australia
[2] Laboratoire des Sciences de l'Environnement Marin (LEMAR), UMR 6539 CNRS UBO IRD IFREMER –Institut Universitaire Européen de la Mer, Technopôle Brest-Iroise, Rue Dumont d'Urville, 29280 Plouzané, France
[3] Institut de Biologie Physico-Chimique, Laboratory of Chloroplast Biology and Light Sensing in Microalgae, UMR 7141, Centre National de la Recherche Scientifique (CNRS), Sorbonne université, 75005 Paris, France
[4] Immunobiotechnology for Aquaculture Group, Department of Cell Biology and Histology, Faculty of Biology, Regional Campus of International Excellence "Campus Mare Nostrum", University of Murcia, 30100 Murcia, Spain
* First co-authors

Corresponding authors: Marc Long (+336 87 97 26 94, marc.florian.long@gmail.com) & Benjamin Bailleul (+331 58 41 51 01, bailleul@ibpc.fr)

Abstract

Allelopathy is an efficient strategy by which some microalgae can outcompete other species. Allelochemicals from the toxic dinoflagellate *Alexandrium minutum* have deleterious effects on diatoms, inhibiting metabolism and photosynthesis and therefore giving a competitive advantage to the dinoflagellate. The precise mechanisms of allelochemical interactions and the molecular target of allelochemicals remain however unknown. To understand the mechanisms, the short-term effects of *A. minutum* allelochemicals on the physiology of the diatom *Chaetoceros muelleri* were investigated. The effects of a culture filtrate were measured on the diatom cytoplasmic membrane integrity (polarity and permeability) using flow-cytometry and the photosynthetic performance using fluorescence and absorption spectroscopy. Within 10 minutes, the unknown allelochemicals induced a depolarization of the cytoplasmic membranes and an impairment of photosynthesis through the inhibition of the plastoquinone-mediated electron transfer between photosystem II and cytochrome b_6f. At longer time of exposure, the cytoplasmic membranes were permeable and the integrity of photosystems I, II and cytochrome b_6f was compromised. Our demonstration of the essential role of membranes in this allelochemical interaction provides new insights for the elucidation of the nature of the allelochemicals. The relationship between cytoplasmic membranes and the inhibition of the photosynthetic electron transfer remains however unclear and warrants further investigation.

Keywords: allelochemicals, allelopathy, *Alexandrium minutum*, *Chaetoceros*, photosynthesis, membrane

1 Introduction

Phytoplankton is under constant biotic pressures (e.g. grazing, competition, parasitism, virus), however some species can form dense monospecific blooms, indicating the involvement of defensive strategies. Some species are capable of releasing secondary metabolites that directly affect the physiology of co-occurring protists with which they compete for nutrients and thus allow them to proliferate freely. This competitive strategy is called allelopathy (Granéli and Hansen, 2006) and the mediating agents of these interactions are called allelochemicals. Allelochemical interactions not only have the potential of inhibiting competitors (Xu et al., 2015 ; Driscoll et al., 2016) but can also facilitate mixotrophic behavior (Tillmann, 2003 ; Blossom et al., 2012) and mitigate grazing by heterotrophic dinoflagellates (John et al., 2015). Allelochemicals are produced by various microalgal groups including cyanobacteria, dinoflagellates, prymnesiophytes, rapidophytes or diatoms (Legrand et al., 2003), but they have mainly been reported in toxic species responsible for harmful algal blooms. The species responsible for these harmful blooms are particularly studied according to their negative effects on ecosystems, fisheries or human health. The harmful effects usually come from the production of paralytic, amnesic or diarrheic toxins. Understanding the factors that favor the establishment and the persistence of these harmful algal blooms is essential to predict them, and mitigate their consequences on the environment.

The understanding of allelochemical interactions is hindered by the poor knowledge of the chemical natures and modes of action of allelochemicals. Most allelochemicals remain uncharacterized. If some of the phycotoxins such as karlotoxins (Place et al., 2012) for example, can mediate allelochemical interactions, it is now accepted that the allelochemicals are not necessarily the phycotoxins produced by harmful species. The known phycotoxins are rarely responsible for the allelochemical potencies (Granéli and Hansen, 2006). Allelochemical interactions are usually reported by their negative effects, but the understanding of their mechanisms remains vague. The physiological outcomes of these interactions are reviewed in (Granéli and Hansen, 2006), and include growth inhibition (Pushparaj et al., 1998; Paul et al., 2009; Suikkanen et al., 2011; Chen et al., 2015; Wang et al., 2017 ; Ternon et al., 2018), damages to cell membranes and cell lysis (Tillmann et al., 2007 ; Prince et al., 2008; Ma et al., 2009; Hakanen et al., 2014; Poulin et al., 2018) and inhibition of photosystem II (PSII)

(Tillmann et al., 2007 ; Gantar et al., 2008; Long et al., 2018a; Poulin et al., 2018; Prince et al., 2008; Ternon et al., 2018). Allelochemical interactions are not restricted to a producer – donor interaction, they can alter species composition of the whole community (Hattenrath-Lehmann and Gobler, 2011).

The genus *Alexandrium* is well known for its potential to form dense blooms reaching more than 10^7 cells L^{-1} (Garcés et al., 2004 ; Chapelle et al., 2015) with deleterious effects on marine wildlife, resources or humans especially through the production of paralytic shellfish toxins (Cembella et al., 2002 ; Anderson et al., 2012;Álvarez et al., 2019). This genus also displays allelochemical potency, which is probably amongst the most studied one within marine phytoplankton. Allelochemical interactions are not mediated by these phycotoxins nor cycloimines but by some unknown extracellular compounds (Arzul et al., 1999; Tillmann and John, 2002 ; Fistarol et al., 2004; Tillmann et al., 2007, Long et al 2018a, 2018b) that can also affect marine resource such as fish or shellfish (Borcier et al., 2017; Bianchi et al., 2019; Castrec et al., 2020, 2019, 2018). The nature of allelochemicals remains mostly unknown. To date, only one putative compound has been identified (Satake et al., 2019) but its activity still has to be confirmed.

Allelochemicals produced by *Alexandrium* spp. induced membrane disruption, modification of membrane biochemistry, inhibition of photosynthesis and esterase activity, increased production of reactive oxygen species (Tillmann et al., 2007 ; Lelong et al., 2011a; Ma et al., 2011; Flores et al., 2012; Long et al., 2018a) in co-occurring protists. However, the sequence of these physiological responses remains unknown, in part because of the use of different algal couples: *Alexandrium minutum*/*Chaetoceros muelleri* (Lelong et al., 2011a; Long et al., 2018a, 2018b), *Alexandrium catenella* (formerly group I of the *A. tamarense/fundyense/catenella*)/*Rhodomonas salina* (Ma et al., 2011), *Alexandrium tamarense* compex/*Tiarina fusus*; *Alexandrium tamarense* complex/*Polykrikos kofoidii* (Flores et al., 2012). For instance, disruption of membranes was shown for *A. catenella* on a cryptophyte (Ma et al., 2011), but was not investigated for *A. minutum*. The inhibition of PSII in allelochemical interactions is probed in a quasi-routine manner simply because PSII activity is easy to measure with the very sensitive and widespread fluorescence techniques. A modification of the integrity of the PSII has been reported for diatoms in the presence of *A. minutum* filtrate (Lelong et al., 2011a; Long et al., 2018b), and in other allelochemical interactions (Hagmann and Jiittner, 1996; Tillmann et al., 2007 ; Prince et al., 2008). Allelochemicals could specifically target and inhibit PSII. Alternatively, the inhibition could be an indirect effect resulting from an inhibition

elsewhere in the photosynthetic electron transfer chain (ETC) or outside of the plastid. Indeed, the inhibition of any step in the ETC leads to a more reduced ETC, which in turn increases the probability of PSII photo-inhibition.

From these observations, several questions arise regarding the mechanism and cellular targets of *A. minutum* allelochemicals. In this frame, this work aims at answering two questions: Do those allelochemicals target first and/or specifically thylakoid membranes and photosynthetic activity? Is the inhibition of photosynthesis a collateral damage following the disruption of cellular membranes including cytoplasmic ones? Therefore, the specific effects of allelochemicals produced by *A. minutum* were investigated on photosystems, photosynthesis activity and cytoplasmic membranes of the common diatom *Chaetoceros muelleri*, co-occurring in the field with *A. minutum* (Chapelle et al., 2014). Allelochemicals were isolated from *A. minutum* cultures by filtration to specifically focus on allelochemical interactions and avoid interference of cell-cell interactions. The short-term effects of a pulse of allelochemicals on photosynthetic and cytoplasmic membranes of *C. muelleri* were investigated by absorption and fluorescence spectroscopy and flow-cytometry, respectively.

2 Materials and methods

2.1 Microalgal cultures and reproducibility between laboratories

A strain of *Alexandrium minutum* (strain CCMI1002, isolated in Ireland and obtained from the Culture Collection of the Marine Institute of Galway), not producing paralytic shellfish toxins (Castrec et al., 2018), was selected according to its high allelochemical potency (Long et al., 2018a). A strain of *Chaetoceros muelleri* (strain CCAP 1010-3 obtained from the CCAP culture collection, formerly listed as *Chaetoceros neogracile* or *Chaetoceros* sp.) was selected because of its sensitivity to *A. minutum* allelochemicals (Borcier et al., 2017; Lelong et al., 2011a; Long et al., 2018a) and its co-occurrence in the field with *A. minutum* (Chapelle et al., 2014). Cells of *A. minutum* were grown in autoclaved synthetic ocean seawater (Morel et al., 1979) supplemented with L1 (Guillard and Hargraves, 1993) medium (salinity = 35 psu, pH = 8.4). Cultures of the diatom *C. muelleri* were grown in filtered (0.2 µm) natural seawater supplemented with L1 medium (salinity = 35 psu, pH = 8.4) and silicate (1.06×10^{-4} M). The natural seawater used for culturing *C. muelleri* was filtered over a carbon filter to retain organic compounds that could possibly inhibit microalgal growth and interfere with *A. minutum* allelochemicals in this study. All cultures were maintained under exponential growth under a

12/12 h light/dark cycle in similar conditions: at 18°C at a light intensity of 30 µmol photon m^{-2} s^{-1} (LUMILUX T8 L 36W/965 BIOLUX) in Brest laboratory, and at 19°C at a light intensity of 38 µmol photons m^{-2} s^{-1} (OSRAM L 30W/640) in Paris laboratory. Cultures were not axenic but were handled under sterile conditions to minimize additional bacterial contamination.

Despite slight differences in the growth conditions, the reproducibility of the photosynthesis performances between the two laboratories was verified. Indeed, the light dependency of photosynthesis, with and without *A. minutum* filtrate, was measured both in Paris and in Brest. No significant difference was observed, confirming that the effect of the supernatant of *A. minutum* on the photosynthetic physiology of *C. muelleri* was the same in both laboratories. The photosynthesis (ETR_{PSI}, Φ_{PSI}, ETR_{PSII}, Φ_{PSII}, photochemical rate) versus intensity data presented in the manuscript are averages of measurements made in the two laboratories. In-depth photosynthesis analysis and flow cytometry investigation of cytoplasmic membranes were then performed in Paris and Brest, respectively. All the raw data used in this manuscript are available at http://www.ibpc.fr/UMR7141/

2.2 Counts of microalgal cells and preparation of filtrate

Counts of microalgal cells were performed using a cell counter (Beckman Coulter, Z2 Cell and Particle Counter) or a FACScalibur (BD Biosciences, San Jose, CA, USA) flow-cytometer equipped with a 488 nm argon laser, red (red emission filter long pass, 670 nm) and green (green emission filter band pass, 530/30nm) fluorescence detectors. Counts with the flow-cytometer were estimated according to flowrate (Marie et al., 1999). Cell variables, e.g. forward scatter (Forward scatter, FSC), side scatter (Side scatter, SSC) and red auto-fluorescence were used to select microalgal populations.

Filtrates were prepared with 0.2 µm syringe filters (Minisart, 16534-K, Sartorius) with an acetate cellulose membrane to avoid any loss of allelochemicals on the membrane (Lelong et al., 2011a). The filtrate concentrations were expressed as cell concentration (cells ml^{-1}) based on the initial culture concentration prior to filtration.

2.3 Inhibitors

To study the photosynthetic transient, several inhibitors were used. 3-(3,4-dichlorophenyl)-1,1-dimethylurea (DCMU) is an inhibitor of the electron transfer to plastoquinone in the Q_B pocket of PSII, 2,5-dibromo-3-methyl-6-isopropyl benzoquinone (DBMIB) is a quinone analogue,

which inhibits the cytochrome b_6f by competitive inhibition at the Q_0 site and carbonyl cyanide m-chlorophenyl hydrazone (CCCP) is an uncoupler that inhibit that suppress trans-thylakoidal proton motive force (pmf). DCMU, DBMIB and CCCP were obtained from Sigma-Aldrich and dissolved in ethanol. Hydroxylamine (HA) is an artificial electron donor to PSII, whereas methylviologen (MV) is an artificial PSI electron acceptor. Both HA and MV were dissolved in water. DCMU, DBMIB, MV and CCCP were used at a final concentration of 10 µM, 0.5 µM, 1 mM and 100 µM, respectively. The combination of 15 µM DCMU and 150 µM HA were used to fully suppress PSII activity (Bailleul et al., 2010), because those concentrations suppressed all the variable fluorescence.

2.4 Photosynthesis measurements

For photosynthesis measurements, cultures of *C. muelleri* in exponential growth phase, at 1-2 10^6 cells mL^{-1}, were concentrated by centrifugation (4500 rpm, 4 min) and resuspended in its own supernatant to reach a final concentration in the range of 5 10^6 to 10^7 cells mL^{-1}. The centrifuged samples were then left ~30 minutes to allow the cells to recover from centrifugation. The filtrate of *A. minutum* was obtained from an initial culture within the range of 18 10^3 to 22 10^3 cells mL^{-1}. After adding the filtrate of *A. minutum* (or the filtrate of *C. muelleri* for the control), flasks were incubated for 10 minutes prior to measurements (otherwise stated).

For measurements of photosynthetic parameters, a Joliot-type spectrophotometer (JTS-10, Biologic, Grenoble, France) equipped with a white probing LED (Luxeon; Lumileds) and a set of interference filters (3–8 nm bandwidth) was used. The device combines absorbance and fluorescence spectroscopy measurements, allowing us to study in the same conditions, on the same sample, the activities of the two photosystems independently, as well as the photochemical rate (which reflects the additive activities of both photosystems, see below), the redox changes of the electron carriers or the pmf. A schematic view of the photosynthetic measurements performed in this work are presented in (Fig. 1). The actinic light was provided by a crown of red-light emitting diodes (LED) (619 nm) or by a dye laser at 690 nm. The red actinic light was chosen to correspond to the minimum of absorption in diatoms and ensure homogeneous light condition in the cuvette. In the fluorescence spectroscopy mode, the JTS-10 was equipped with a white probing LED (Luxeon; Lumileds) and a blue filter (470 nm) for detecting pulses. The cut-off filter on the measuring photodiode is a LPF650 + RG 665 from Schott (Mainz, Germany) and on the reference side is a BG39 filter from Schott. In the

absorption mode, the cut-off filters were the same on measure and reference photodiodes (BG39 for ECS measurements and a high pass RG695 for P700 measurements). In absorption mode, the absorption changes induced by the measuring flashes alone (in the absence of actinic light) were subtracted from those recorded in presence of actinic light for every trace to eliminate small artifacts due to measuring flashes.

Fluorescence spectroscopy. PSII parameters were calculated as described in (Genty et al., 1989). Maximum quantum yield of PSII was calculated as $F_v / F_m = (F_m-F_0)/ F_m$, where F_0 is the fluorescence of the dark-adapted (1 minute) sample and F_m the fluorescence when a saturating pulse is applied on dark-adapted sample. Quantum yield in light-adapted samples of PSII (Φ_{PSII}) was calculated as $\Phi_{PSII}= (F_m'-F_{stat})/F_m'$, where F_{stat} is the fluorescence of the sample adapted to the actinic light and Fm' the fluorescence when a saturating pulse is applied on light-adapted sample. The electron transport rate through PSII (ETR_{PSII}) was normalized to the maximal value in the control at 800 µmol photons m^{-2} s^{-1} to focus on filtrate-induced changes and corrected for variations in the initial photosynthetic physiology of *C. muelleri*. It was calculated as $ETR_{PSII} = \Phi_{PSII} * I / (\Phi_{PSII\text{-}800} * 800)$, where I is the actinic light irradiance.

Fluorescence induction kinetic was performed at room temperature using a DeepGreen Fluorometer (JbeamBio, France) with samples that were dark-adapted for 1 minute before measurements (Rappaport et al., 2007).

P700 measurements. For photosystem I (PSI) parameters, the redox state of the PSI primary donor (P_{700}) was calculated as the difference between the absorption changes kinetic at 705 nm and 735 nm, to eliminate spectrally flat contributions due to diffusion. Properties of PSI were calculated from the measurements of the absorption changes in the dark (P_0), in the light-adapted condition (P_{stat}) and after a saturating pulse (P_{sp}). The quantum yield of PSI (Φ_{PSI}), the donor side (Y(ND)) and acceptor side (Y(NA)) limitations were then calculated according to (Klughammer and Schreiber, 2008).

$$\Phi_{PSI} = (P_{sp} - P_{stat}) / (P_{max} - P_0)$$

$$Y(ND) = (P_{stat} - P_0) / (P_{max} - P_0)$$

$$Y(NA) = (P_{max} - Psp) / (P_{max} - P_0)$$

All data were normalized to $P_{max} - P_0$ (corresponding to 100% oxidized P_{700}), P_{max} being the absorption change after a saturating pulse in the presence of the PSII inhibitor DCMU. The

electron transport rate through PSI (ETR_{PSI}) was normalized to the maximal value of the control at 800 µmol photons m^{-2} s^{-1} (like for ETR_{PSII}) and calculated as $ETR_{PSI} = \Phi_{PSI} * I/(\Phi_{PSI\text{-}800} * 800)$, where I is the actinic light irradiance.

Measurement of linear and quadratic ECS spectra. To obtain the spectra of the linear and quadratic Electro-Chromic Shift (ECS) signals in *C. muelleri*, a strong electric field was generated by shining a 10 ms saturating pulse (red light, 619 nm, 6000 µmol photons m^{-2} s^{-1}). Then the approach described in (Bailleul et al., 2015) was used to deconvolute the two ECS components during the relaxation of the electric field. In brief, the kinetics of the absorption changes following the pulse was followed, removing the first 50 ms after the pulse (additional signals like the ones associated to the redox changes of the c-type cytochromes are then relaxed). The ECS decay kinetics was then fitted as a sum of a linear and a quadratic component, which allowed to reconstruct the two spectra. Cells were treated with 100µM of the uncoupler CCCP to ensure that no trans-thylakoidal electric field was present in the dark-adapted sample, prior to the pulse.

Determination of the appropriate wavelengths for measurements. The linear and quadratic ECS spectra revealed that 520 nm and 564 nm are convenient wavelengths, where only linear and quadratic signals contribute to ECS, respectively. On that basis, a three wavelengths deconvolution was performed to obtain contributions from linear ECS, quadratic ECS and c-type cytochromes (Cyt c). The latter was calculated as:

Cyt c= [554] – 0.35* [520] – 0.5 * [564], where [554], [520] and [564] are the absorption difference signals at 554 nm, 52 0 nm and 564 nm, respectively.

Then, the linear ECS (ECSlin) was calculated as ECSlin = [520] – 0.25 * Cyt c, and the quadratic ECS (ECSquad) was calculated as ECSquad = [554] + 0.15 * Cyt c.

Flash-induced ECS kinetics. The ECS kinetics following a single turnover of both photosystems were measured using a 6 ns saturating laser flash provided by a dye laser at 690 nm. Then the kinetics of flash-induced ECS and cytochromes redox changes were calculated using the deconvolution procedure described above. The linear ECS signal at the first point (measured shortly -160 µs- after the flash) provides the contribution to the electric field of 1 charge separation per photosystem (used for normalization, see below). The rate of re-reduction of c-

type cytochromes and the rate of ECS decay were calculated as the time constant of the mono-exponential extrapolation of the c-type cytochromes and ECS relaxation kinetics, respectively.

Photochemical rates. The photochemical rate (rate at which PSI and PSII perform charge separations) was calculated from ECS measurements as described in (Bailleul et al., 2010). Briefly, under steady-state illumination, the ECS signal results from positive contributions to the transmembrane potential from PSII, the cytochrome b_6f complex and PSI (which contribute to the net movement of positive charges from the stroma to the lumen, increasing the electric field), as well as the negative one by the chloroplastic ATP synthase (moving protons out of the lumen). Because only PSI and PSII use light as a substrate, the change of slope of the ECS immediately after turning off the light is a direct measurement of the photochemical rate, i.e. the rate at which PSI and PSII were performing charge separations under illumination. The slope of ECS was measured for the first 5 ms after light offset and then normalized by the laser flash induced ECS increase, providing an expression of the photochemical rate in charge separations per photosystem per second (charge sep. PS^{-1} s^{-1}). Like for ETR_{PSII} and ETR_{PSI}, data were normalized to the maximal value in the control at 800 µmol photons m^{-2} s^{-1}.

2.5 Flow-cytometric (FCM) measurements

The *A. minutum* filtrate (from a culture at 20 000 ± 2 000 cells mL^{-1}) used for flow-cytometry was checked for some photosynthesis measurements in parallel, to ensure that those experiments were made in the same conditions of inhibition than the ones focusing on the mechanism of photosynthetic inhibition. For FCM measurements, cultures of *C. muelleri* were diluted 10 times with their own filtrate to reach a final concentration around 200 000 cells mL^{-1}.

Cytoplasmic membrane potential. Modifications of the cytoplasmic membrane potential were assessed using an EasyCyte Plus cytometer (Guava Technologies, Millipore, Billerica, MA, USA) equipped with a 488-nm argon laser and red (680, 30 nm bandwith) and green (525 nm, 30 nm bandwidth) fluorescence detectors. To estimate the relative depolarization of cytoplasmic membranes, cells were stained with Bis-(1,3-Dibutylbarbituric Acid) Trimethine Oxonol, $DiBAC_4(3)$ (Molecular Probes, Eugene, OR, USA) for 10 min at a final concentration of 0.97 µM. $DiBAC_4(3)$ is a fluorescent probe emitting at 516 nm that can enter cells with depolarized cytoplasmic membranes (Seoane et al., 2017). Once inside the cells, $DiBAC_4(3)$

binds to intracellular proteins and membranes. The amount of protein-bound $DiBAC_4(3)$ is dependent on the cytoplasmic membrane potential (Bräuner et al., 1984). Cells with an increased depolarization (increase in the membrane potential) of their cytoplasmic membrane exhibit an increase in their internal fluorescence (proportional to the accumulation of dye within the cell). To obtain a positive control (cells with depolarized membranes), *C. muelleri* cell membranes were depolarized with digitonin (30 min incubation, final concentration of 40 µg mL^{-1}), a weak non-ionic detergent (Prado et al., 2012). The relative depolarization of membranes was expressed as the mean fluorescence value of the cell population. After checking the homoscedasticity and the normality of data, the significant differences in the $DiBAC_4(3)$ fluorescence between *C. muelleri* from the control or exposed to the filtrate, for 10 min or 30 min, were compared with a Student t-test.

Membrane permeability. Measurements of membrane permeability were performed on a FACSCalibur flow-cytometer. The membrane permeability was assessed with SYTOXGreen (Molecular Probes, Eugene, OR, USA), a fluorescent probe (523 nm) that cannot cross cell membranes unless membrane integrity is compromised according to manufacturer and several studies (Brussaard et al., 2001; Lelong et al., 2011b; Naghdi et al., 2016). Once inside the cell, the probe binds to DNA and forms a fluorescent dye. Thus, only cells that lost their membrane integrity (i.e. became permeable) become fluorescent. Samples were stained with SYTOXGreen for at least 10 min at a final concentration of 0.05 µM (Koppel et al., 2017). Membrane permeabilization was expressed as the percentage of fluorescent cells. After checking for homoscedasticity and normality of data, the significant differences in the percentage of cells permeable to SYTOXGreen between *C. muelleri* from the control or exposed to the filtrate were compared with a Student t-test.

3 Results

3.1 A strong inhibition of photosynthetic activity by A. minutum filtrate

In order to assess the effect of *A. minutum* filtrate on the photosynthetic activity of *C. muelleri*, the overall activity of photosynthesis was first measured at different irradiances. This was performed using the electro-chromic shift (ECS) of photosynthetic pigments (Witt, 1979). In *C. muelleri*, like in other diatoms (Bailleul et al., 2015) and pinguiophytes (Berne et al., 2018), the ECS is the sum of a linear and a quadratic component, which have been deconvoluted as

described in the Methods section (Fig. 2A and B). The deconvolution allowed the extraction of pure linear and quadratic components, as demonstrated in (Fig. 2C).

The linear ECS is proportional to the electric field generated by the photosynthetic process and can be used to measure the overall photosynthetic activity (Bailleul et al., 2010). Indeed, the change of slope of the ECS immediately after turning off the light (Fig. 3A) was a direct measurement of the photochemical rate (see Material and Methods, 2.4). In the control, the photochemical rate increased with light irradiance (Fig. 3B), as expected, and did not reach saturation at 800 µmol photons m^{-2} s^{-1} in agreement with the spectral characteristics of the illumination (low light absorption by diatoms, see Material and Methods, 2.4). In the presence of *A. minutum* filtrate, the slope of the ECS after turning off the light was drastically reduced (Fig. 3A), resulting in an almost full inhibition of *C. muelleri* photochemical rates at all light intensities (Fig. 3B).

The very strong inhibition of the photochemical rate by the filtrate of *A. minutum* suggested that both the activities of the linear electron flow (from water to PSI acceptors) and the cyclic electron flow around PSI ((Shikanai, 2007) and see Fig. 1), a process whose extent is still debated in diatoms (Falciatore et al., 2020), were suppressed by the allelochemicals of *A. minutum*. To further confirm this hypothesis, the activities of PSII and PSI in the diatom (Fig. 4) were measured under the same illumination conditions. The activity of PSII reflects the efficiency of the linear process only, whereas PSI activity is the sum of the linear and cyclic pathways. The quantum yield of PSII (Φ_{PSII}) was measured with fluorescence spectroscopy and the quantum yield of PSI (Φ_{PSI}) with P700 absorption measurements (Fig. 4A and B, see Methods). As expected, both the quantum yields of PSII (Fig. 4C) and PSI (Fig. 4D) decreased with light irradiance in the control sample, because of the progressive reduction of PSII acceptors and oxidation of PSI donors with increasing light (Falkowski and Raven, 2007). However, at all light irradiances, the quantum yields of both photosystems were significantly lower in the presence of *A. minutum* filtrate (Fig. 4C and D). In the control, the light dependence of the electron transfer rate through PSII (ETR_{PSII}, Fig. 4E) and photochemical rate (Fig. 3B) were very similar. The filtrate of *A. minutum* almost fully inhibited ETR_{PSII}, which confirmed that it hampered the linear electron flow. PSI electron flow rate (ETR_{PSI}) was also almost fully suppressed in the presence of filtrate of *A. minutum* allelochemicals (Fig. 4F). This confirmed that both linear and cyclic electron flow rates were very low in the presence of *A. minutum* filtrate.

3.2 The first target of A. minutum was a non-photochemical step of photosynthesis.

Such a complete suppression of photosynthetic activity under steady state illumination could be due to the specific inhibition of any of the photosynthetic steps, i.e. at the level of photosynthetic complexes (PSII, PSI, cytochrome b_6f, ATPase), or an impairment of the diffusion of the electron carriers transferring electrons from one photosynthetic complex to another (e.g. plastoquinones or cytochrome c_6) or an inhibition of the Calvin-Benson-Bassham cycle. One could imagine that the photosystems themselves were inhibited by the allelochemicals. Indeed, an inhibition of the maximal quantum yield of PSII (F_v/F_m) was shown to occur within 30 minutes in these conditions (Long et al., 2018b) and this inhibition was even proposed as a bioassay for these allelopathic interactions (Long et al., 2018a). In agreement with that, a strong inhibition of both PSII and PSI activities was observed at the end of the measurements, in the exposed samples only. The F_v/F_m decreased by ~50 % and the total amount of photo-oxidizable P700 (P_{max}) decreased by ~75 % at the end of the experiment (Sup Fig. 1). However, neither PSI nor PSII activities were inhibited at the beginning of the experiment (highlighted by the similar yields of PSII and PSI in the dark in absence or presence of *A. minutum* filtrate; Fig. 4C and D), whereas the inhibition of the photosynthetic activity in the light occurred immediately, from the first light step, as observed for the photochemical rate, ETR_{PSII} or ETR_{PSI} (Fig. 4E and F). In order to confirm that the suppression of the photosynthetic activity was not due to photosystems inhibition, another experiment was performed to measure the quantum yield of both PSI and PSII in the dark and in moderate light, with the two measurements performed in close succession. This experiment showed that the activities of both PSI and PSII in the presence of light were already suppressed in the presence of *A. minutum* filtrate (Fig. 5A) in conditions where PSI and PSII integrity (maximal efficiencies) were unaffected (Fig 5B), demonstrating that the *A. minutum* filtrate inhibited photosynthetic activity by targeting a non-photochemical step first.

3.3 The photosynthetic inhibition occurred between PSII and PSI

Our results lead to two possibilities. The allelochemicals could have affected the electron transfer from Q_A, the first quinone acceptor in PSII, to P700 at the PSI level - this part of the photosynthetic chain provides electrons to PSI and is therefore usually referred to as the donor side of PSI. Alternatively, they could have modified the electron transfer from ferredoxins to the carbon fixation in the Calvin-Benson-Bassham cycle and other alternative pathways - this part of the photosynthetic chain is fueled by electrons from PSI and is therefore usually referred

to as the acceptor side of PSI. To distinguish between these two possibilities, the acceptor (Y(NA)) and donor (Y(ND)) side limitation of PSI (see Methods) were measured under the same illumination. The data clearly showed that the decrease of PSI quantum yield (Φ_{PSI}) was due to an increase in the donor side limitation in the treated sample (Fig. 5A). In other terms, a lower proportion of PSI centers was open (and participating to electron transfer) because of a higher percentage of oxidized P700 in the light ($P700^+$, ~70% in the treated sample vs ~20% in the control at the highest intensity). This indicated that the inhibition occurred between PSII and PSI, and not on the acceptor side of PSI. To further confirm this, the artificial PSI electron acceptor, methylviologen (MV, or paraquat), was used to release acceptor side limitation by providing an efficient sink to electrons from PSI. In agreement with the Y(ND) and Y(NA) measurements, the addition of 1 mM MV did not modify the activities of PSII or PSI, neither in the control nor in the treated sample (Fig. 5A). Together, these results indicated that the first site of inhibition of the photosynthetic electron transfer chain took place between Q_A and P700.

3.4 The first photosynthetic target of A. minutum was the thylakoid membrane (electron transfer from PSII to b6f)

To determine the primary target of the unknown secondary metabolite(s) produced by *A. minutum*, the ECS kinetics following a saturating laser flash (Fig. 6) was used to probe the activity of each photosynthetic complex (PSI, PSII, b_6f, ATPase). Indeed, the photosystems and cyt b_6f participate in the generation of the electric field, by moving protons (positive charges) inside the lumen, whereas the ATPase neutralizes this electric field by moving the protons back to the stroma (Bailleul et al., 2010). The redox changes of the c-type cytochromes (cytochrome *f* and cytochrome c_6) were also measured as described in Methods. The results are shown in (Fig. 6) for diatom cells alone or 10 min after adding *A. minutum* filtrate. After a saturating laser flash, three distinct phases are typically observed (Joliot and Delosme, 1974).

i) Right after the flash (here 160µs) all photosystems I and II perform one (and only one) charge separation (Fig. 6A), increasing the electric field by as much ("a phase"). The similar "a phase" in control and exposed cells confirmed that the photochemical events at PSII and PSI level were not the direct targets of the allelopathic compound(s) (first time point after the flash, panel A). These charge separations corresponded to the electron transfer from water to the Q_A pocket in PSII and from P700 to ferredoxins at the PSI level. At the same time point, a similar

oxidation of the c-type cytochromes (cytochromes c_6 in the lumen and cytochrome *f*) was observed in control and exposed cells (panel B). This means that regardless of the exposure to the filtrate or not, the transfer from c-type cytochromes to P700 was faster than 160 µs.

ii) The second phase ("b phase", ~10 ms) corresponds to the electron transfer from plastoquinols to c-type cytochromes catalyzed by the cytochrome b_6f (Fig. 6B). The filtrate did not affect this phase, since the re-reduction of c-type cytochromes was not significantly modified by the filtrate. The proton pumping activity of the cytochrome b_6f, the "b phase" should have given a second rise of the electric field (Joliot and Delosme, 1974) but here this phase was partly hidden by the fast activity of the ATPase.

iii) The last phase of ECS kinetics ("c phase") corresponds to the consumption of the flash-induced proton motive force (pmf) by the ATPase, resulting in the relaxation of the ECS (Fig. 6C). This phase did not seem to be affected by *A. minutum* filtrate.

The quadratic ECS increase right after the flash was significantly reduced in the exposed cells, suggesting that the pmf in the dark was affected by *A. minutum* filtrate. This aspect will be discussed later (see Discussion). The unaffected oxidation and reduction of c-type cytochromes revealed together a normal electron transfer from the plastoquinol in the Q_O pocket of the cytochrome b_6f to P700. These results, together with the previous results indicating that the limitation occurred between Q_A and P_{700}, pointed to a limitation of the electron flow between the Q_A pocket in PSII and the Q_O pocket in b_6f.

To confirm this and get further insight into the mechanism of inhibition, the fluorescence induction and relaxation kinetics were measured (see Methods). The protocol consisted in the measurement of the F_0 parameter in the dark, followed by 500 ms of low light illumination (fluorescence reaches F_{stat}). Then a saturating pulse was applied to reduce all plastoquinones and quinone pockets (F_m is measured) and the kinetics of relaxation of the fluorescence is measured in subsequent darkness. The latter phase of fluorescence relaxation (from F_m to F_0) reflected the re-oxidation of Q_A, i.e. the electron transfer from this quinone pocket in PSII to the oxidized components of the ETC at the end of the saturating pulse, i.e. cofactors in the cytochrome b_6f, cytochromes c_6 or P700. The slowing down of this phase after exposition to the filtrate therefore confirmed that the treatment with *A. minutum* supernatant impaired the electron transfer from Q_A to PSI donors (Fig. 7A). The phase of fluorescence increase was more

informative. When the light was turned on in the control, fluorescence increased in <100 ms and reached a steady state value before the saturating pulse was applied. In the presence of the filtrate, after a first increase, which was similar to the one observed in the control, a second increase of fluorescence occurred in the 100 to 400 ms time range, which reflected an over-saturation of the ETC (Fig. 7A). The increase kinetics could be compared to the one of the control with DCMU (10 µM), an inhibitor of Q_B pocket of PSII, and DBMIB (0.5 µM), an inhibitor of the cytochrome b_6f. In both cases, a strong increase of the stationary fluorescence was observed, but the kinetics were different: in DCMU conditions, PSII can perform only one charge separation before Q_A is fully reduced and reaches F_m very fast, whereas in DBMIB conditions, Q_B and the whole plastoquinol pool must be reduced before Q_A becomes fully reduced and fluorescence reaches F_m with a slower kinetics. The comparison between the fluorescence induction curve in the presence of the filtrate and in the presence of DCMU indicated that the inhibition of photosynthesis was not at the Q_B level; the effect of the filtrate is indeed closer to the one of DBMIB (Fig. 7B). This experiment ruled out the possibility that the inhibition step is in vicinity to PSII and therefore points towards an inhibition at the level of the PQ pool and/or its interaction with the cytochrome b_6f.

Altogether, at short time of exposure (10 min) with *A. minutum* filtrate, PSII and PSI were fully functional (Fig. 4 and Fig. 5) and the electron transfer from Q_0 in the b_6f to P_{700} was unaffected (Fig. 5). Simultaneously, the overall photosynthetic activity (measured via three different techniques: fluorescence P700 or ECS measurements) was decreased by 80-90%. These results pointed out a primary target of *A. minutum* on the photosynthetic apparatus of *C. muelleri* at the level of the electron transfer between Q_B in PSII and Q_O in b_6f, i.e. the diffusion of the plastoquinol/plastoquinone in the thylakoid membrane or its docking to/release from the cytochrome b_6f. This conclusion is in agreement with the rise of fluorescence kinetics at the onset of light, as well as the re-oxidation of Q_A kinetics.

3.5 A degradation of the whole photosynthetic apparatus was observed at longer incubation times

To get a more complete view of the time response of the photosynthetic apparatus to the exposure to *A. minutum* filtrate, the flash-induced ECS and c-type cytochrome redox kinetics were measured at different exposure times (10, 40 and 90 minutes), in parallel to photochemical rate measurements (Fig. 8). In the control cells, the flash-induced ECS kinetics and the

photochemical rate were the same at the three time points, which indicated that the overall photosynthetic characteristics and performance were constant over time. Again, 10 min exposure did not affect the photosystem capacities (« a phase » of ECS, Fig. 8E), the oxidation and reduction of c-type cytochromes (Fig. 8B and C) or the activity of the ATPase (ECS relaxation, Fig. 8F). Only the photochemical rate (Fig. 8A) and the quadratic-to-linear ratio (Fig. 8D, see Discussion) were strongly reduced. At longer time of exposure (40 and 90 min), the photochemical rate (Fig. 8A) and quadratic-to-linear ratio (Fig. 8D) remained lower in the treated cells, whereas a decrease of PSI and PSII efficiencies (Fig. 8C and E) appeared, in agreement with previous results based on fluorescence and P700 measurements (Sup Fig. 1). The rate of re-reduction of c-type cytochromes, which reflected the rate of b_6f turnover, also decreased after 40 min of exposure to *A. minutum* filtrate (Fig. 8C). These results highlighted an overall degradation of the photosynthetic apparatus (PSI, PSII, b_6f) as time of exposure increases.

3.6 A modification of membranes

The inhibition of the electron transfer chain was due to a problem in the quinone-mediated electron transfer between Q_B to the quinone-binding site Q_O in the cytochrome b_6f in the thylakoid membrane. Given that allelochemicals from *A. catenella* caused the disruption of membranes that led to lytic activity (Ma et al., 2011), a disruption of membranes could also take place with *A. minutum* allelochemicals. In other words, are *A. minutum* allelochemicals disrupting all cellular membranes? Flow-cytometry analysis revealed that *A. minutum* filtrate induced a strong depolarization of cytoplasmic membranes of more than 95% of *C. muelleri* cells within only 10 min (Fig. 9A). Only metabolically active cells with no damages to membranes can maintain a normal membrane potential (Jepras et al., 1997; Prado et al., 2012). Depolarization of membranes can originate from membrane permeabilization or from an inhibition of the energy metabolism. This strongly suggests that the depolarization of membranes represents an early signal of membrane disruption as the uncoupling agent eliminated the proton gradient. Simultaneously, a significant, but small increase in the percentage of cells with permeable cytoplasmic membranes as compared to the control could be observed at 10 min (Fig. 9B). This was later confirmed by the strong increase in the percentage of cells with permeable membranes after 30 minutes of exposure (Fig. 9B).

4 Discussion

This study reveals that the (thylakoid and cytoplasmic) membranes are amongst the first physiological targets of allelochemicals from *A. minutum*. Two distinct phases were observed, allowing us to identify "primary" targets from the side effects of filtrate exposure, and to hypothesize the cascades of events occurring within the different membranes of *C. muelleri*.

In the first phase (within the first 10 min), a general depolarization of cytoplasmic membranes and permeabilization of external membranes from few cells were induced in agreement with the mode of action of *A. catenella* allelochemicals on other protists (Ma et al., 2011). A direct effect of *A. minutum* filtrate was also observed on membranes of oyster hemocytes causing membrane permeability (Hégaret et al., 2011). Concomitantly, an inhibition of electron flow between PSII and b_6f was measured. This resulted in a quasi-complete arrest of the photosynthetic electron transfer chain, illustrated by the strong inhibition of the activities of PSII and PSI in the light. It is to note that the inhibition of PSI seemed slightly stronger than the one of PSII. This could reflect the presence of some cyclic electron flow in the control conditions and its full suppression in the presence of *A. minutum* filtrate. Another fast response of photosynthesis to the allelochemicals was the suppression of the quadratic ECS increase right after the flash. This parameter is difficult to interpret, as it depends both on the electric field generated by PSII and PSI charge separations and on the pre-existing electric field (Joliot and Joliot, 1979 ; Bailleul et al., 2010). In contrast, the linear ECS increase only depends on the electric field generated by PSII and PSI after the saturating laser flash. Theoretically, the ratio of the quadratic-to-linear ECS is a direct measurement of the pre-existing electric field, the electric component of the pmf (Bailleul et al., 2010, 2015; Dow et al., 2020). This ratio was significantly reduced in the exposed cells, suggesting that the pmf in the dark was affected by *A. minutum* filtrate. This can be due to an inhibition of mitochondrial respiration or to an uncoupling effect of the secondary metabolites that affect mitochondria, the chloroplast, or both (Bailleul et al., 2015). A partial inhibition of *C. muelleri* respiratory activity in response to *A. minutum* filtrate was observed before (Lelong et al., 2011a), but this inhibition developed slowly, compared to the fast suppression of the pmf measured in this work. For this reason, the hypothesis of an uncoupler effect seems more plausible and should be tested in future investigations.

After longer times of exposure, the membranes of *C. muelleri* seemed to become much more affected by *A. minutum* allelochemicals. Cytoplasmic membranes appeared more permeable,

suggesting that the loss of membrane polarization could be attributed to pores in the membranes that became larger or more numerous with longer exposure time. Meanwhile, in the photosynthetic membranes, strong inhibitions of PSI and PSII, and the reduced turnover of the cytochrome b_6f occurred. Results also highlighted that, while PSII can be probed to measure allelochemical potency (Long et al., 2018a), it is not a specific target. These alterations of photosynthetic complexes may be a consequence of the dysfunction of the diffusion of the quinones between Q_B and cytochrome b_6f, leading to the suppression of the photosynthetic electron transport. The overall deleterious effects on the photosynthetic apparatus induced photoprotection mechanisms previously measured in *C. muelleri* exposed to *A. minutum* filtrate (Long et al., 2018b). These defense mechanisms are, however, likely insufficient to counteract the severe damages to the membranes at the *A. minutum* concentration we chose for this study.

The nature of allelochemicals of *A. minutum* still eludes us, but our results provide new insights into the physico-chemical properties expected for candidate molecules. Indeed, the three main consequences of the allelochemicals here (Fig. 10) were 1) the disruption of cytoplasmic membranes, 2) the decrease of the plastoquinone diffusion and 3) the suppression of the electric component of the pmf in the dark-adapted cells. Overall, the mode of action of *A. minutum* allelochemicals is very similar to that of *Karenia brevis*, which alter the membrane integrity, modify the lipidome and compromise photosynthesis of the competing species (Poulin et al., 2018). Membrane biochemical composition varies greatly among eukaryotes. As membranes are amongst the first targets for *A. minutum* allelochemicals, it can be hypothesized that their biochemical composition might drive, at least partially, the sensitivity of species to *A. minutum*. The composition of membranes was already suggested to be an important factor in some allelochemical interactions (Deeds and Place, 2006; Morsy et al., 2008a, 2008b; Ma et al., 2011).

Our study demonstrates that allelochemicals from *A. minutum* have the potential to inhibit photosynthesis and quickly lyse co-occurring protists at environmentally relevant cell densities. Indeed, the concentration of *A. minutum* used in this study (~20 000 cells mL^{-1}) was higher than the half maximal effective concentration inhibiting Fv/Fm of a culture by 50 % measured in previous study (~4 000 cells mL^{-1}; Long et al., 2018) but lower than the maximal concentrations of *A. minutum* measured in the field, which can reach 40 000 cells mL^{-1} (Chapelle et al., 2015) or more (Garcés et al., 2004). The allelochemical potency would favor the establishment of *A. minutum* monospecific bloom by eliminating other microalgae competing for nutrients, by facilitating mixotrophic behavior (already evidenced in this species by (Meng et al., 2019)) and

potentially decreasing the grazing by other dinoflagellates as observed for *A. fundyense* (John et al., 2015). A better description of the biochemistry of planktonic membranes, the chemical elucidation of allelochemicals and a precise identification of their specific targets is essential to identify the potential marine species (not only planktonic) affected by these metabolites. Eventually, these results will help predicting the potential structuring effects of allelochemical interactions on planktonic communities.

Acknowledgments

This study was carried out with the financial support of the Centre National de la Recherche Scientifique, Sorbonne Université, the Région Bretagne, the University of Wollongong and the GDR Phycotox. ML, CGF and HH acknowledge support from the National Research Agency (ANR) ‘‘ACCUTOX’’ project 13-CESA-0019 (2013–2017). AP and BB were supported by the European Research Council (ERC) PhotoPHYTOMICS project (Starting Grant PhotoPHYTOMICS, grant agreement N° 715579). AP had financial support from the French Ministry of Education. The authors would like to warmly thanks Dr. Philippe Soudant, Dr. Géraldine Sarthou, Dr. Francis-André Wollman and Dr. Dianne F. Jolley for the comments on the manuscript, the constructive discussions and english corrections.

Contributions

ML, AP, HH and BB designed the research. ML, AP, CGF, HH and BB performed the research and analyzed the data. ML, AP, HH and BB wrote the first version of the manuscript and all co-authors revised the manuscript. ML and AP contributed equally to this work.

References

Adolf, J., Bachvaroff, T., Krupatkina, D., Nonogaki, H., Brown, P., Lewitus, A., Harvey, H., Place, A., 2006. Species specificity and potential roles of *Karlodinium micrum* toxin. African Journal of Marine Science 28, 415–419. https://doi.org/10.2989/18142320609504189

Álvarez, G., Díaz, P.A., Godoy, M., Araya, M., Ganuza, I., Pino, R., Álvarez, F., Rengel, J., Hernández, C., Uribe, E., Blanco, J., 2019. Paralytic Shellfish Toxins in surf clams *Mesodesma donacium* during a large bloom of *Alexandrium catenella* dinoflagellates associated to an intense shellfish mass mortality. Toxins 11, 188.

Anderson, D.M., Alpermann, T.J., Cembella, A.D., Collos, Y., Masseret, E., Montresor, M., 2012. The globally distributed genus *Alexandrium*: Multifaceted roles in marine ecosystems and impacts on human health. Harmful Algae 14, 10–35. https://doi.org/10.1016/j.hal.2011.10.012

Arzul, G., Seguel, M., Guzman, L., Erard-Le Denn, E., 1999. Comparison of allelopathic properties in three toxic *Alexandrium* species. Journal of Experimental Marine Biology and Ecology 232, 285–295. https://doi.org/10.1016/S0022-0981(98)00120-8

Bailleul, B., Berne, N., Murik, O., Petroutsos, D., Prihoda, J., Tanaka, A., Villanova, V., Bligny, R., Flori, S., Falconet, D., Krieger-Liszkay, A., Santabarbara, S., Rappaport, F., Joliot, P., Tirichine, L., Falkowski, P.G., Cardol, P., Bowler, C., Finazzi, G., 2015. Energetic coupling between plastids and mitochondria drives CO2 assimilation in diatoms. Nature 524, 366–369. https://doi.org/10.1038/nature14599

Bailleul, B., Cardol, P., Breyton, C., Finazzi, G., 2010. Electrochromism: a useful probe to study algal photosynthesis. Photosynthesis research 106, 179–189. https://doi.org/10.1007/s11120-010-9579-z

Berne, N., Fabryova, T., Istaz, B., Cardol, P., Bailleul, B., 2018. The peculiar NPQ regulation in the stramenopile *Phaeomonas* sp. challenges the xanthophyll cycle dogma. BBA - Bioenergetics 1859, 491–500. https://doi.org/10.1016/j.bbabio.2018.03.013

Bianchi, V.A., Langeloh, H., Tillmann, U., Krock, B., Müller, A., Bickmeyer, U., Abele, D., 2019. Separate and combined effects of neurotoxic and lytic compounds of *Alexandrium* strains on *Mytilus edulis* feeding activity and hemocyte function. Fish & Shellfish Immunology 84, 414–422. https://doi.org/10.1016/j.fsi.2018.10.024

Blossom, H.E., Daugbjerg, N., Hansen, P.J., 2012. Toxic mucus traps: A novel mechanism that mediates prey uptake in the mixotrophic dinoflagellate *Alexandrium pseudogonyaulax*. Harmful Algae 17, 40–53. https://doi.org/10.1016/j.hal.2012.02.010

Borcier, E., Morvezen, R., Boudry, P., Miner, P., Charrier, G., Laroche, J., Hegaret, H., 2017. Effects of bioactive extracellular compounds and paralytic shellfish toxins produced by *Alexandrium minutum* on growth and behaviour of juvenile great scallops *Pecten maximus*. Aquatic Toxicology 184, 142–154. https://doi.org/10.1016/j.aquatox.2017.01.009

Bräuner, T., Hülser, D.F., Strasser, R.J., 1984. Comparative measurements of membrane potentials with microelectrodes and voltage-sensitive dyes. Biochimica et Biophysica Acta (BBA) - Biomembranes 771, 208–216. https://doi.org/10.1016/0005-2736(84)90535-2

Brogden, K.A., 2005. Antimicrobial peptides: pore formers or metabolic inhibitors in bacteria? Nature Review Microbiology 3, 238–250. https://doi.org/10.1038/nrmicro1098

Brussaard, C., Marie, D., Thyrhaug, R., Bratbak, G., 2001. Flow cytometric analysis of phytoplankton viability following viral infection. Aquatic Microbial Ecology 26, 157–166. https://doi.org/10.3354/ame026157

Castrec, J., Hégaret, H., Alunno-Bruscia, M., Picard, M., Soudant, P., Petton, B., Boulais, M., Suquet, M., Quéau, I., Ratiskol, D., Foulon, V., Le Goïc, N., Fabioux, C., 2019. The dinoflagellate *Alexandrium minutum* affects development of the oyster *Crassostrea gigas*, through parental or direct exposure. Environmental Pollution 246, 827–836. https://doi.org/10.1016/j.envpol.2018.11.084

Castrec, J., Hégaret, H., Huber, M., Le Grand, J., Huvet, A., Tallec, K., Boulais, M., Soudant, P., Fabioux, C., 2020. The toxic dinoflagellate *Alexandrium minutum* impairs the performance of oyster embryos and larvae. Harmful Algae 92, 101744. https://doi.org/10.1016/j.hal.2020.101744

Castrec, J., Soudant, P., Payton, L., Tran, D., Miner, P., Lambert, C., Le Goïc, N., Huvet, A., Quillien, V., Boullot, F., Amzil, Z., Hégaret, H., Fabioux, C., 2018. Bioactive extracellular compounds produced by the dinoflagellate *Alexandrium minutum* are highly detrimental for oysters. Aquatic Toxicology 199, 188–198. https://doi.org/10.1016/j.aquatox.2018.03.034

Cembella, A.D., Quilliam, M.A., Lewis, N.I., Bauder, A.G., Dell'Aversano, C., Thomas, K., Jellett, J., Cusack, R.R., 2002. The toxigenic marine dinoflagellate *Alexandrium tamarense* as the probable cause of mortality of caged salmon in Nova Scotia. Harmful Algae 26, 1-13.

Chapelle, A., Le Bec, C., Le Gac, M., Labry, C., Amzil, Z., Guillou, L., Dreanno, C., Klouch, K., Siano, R., Pineau, L., Savar, V., Destombe, C., Dia, A., Lazure, P., Petton, S., Plus, M., Le Brun, L., Abernot, C., Duval, A., Doner, A., Gouriou, J., Gal, D. Le, Caradec, F., Andrieux, F., Malestroit, P., 2014. Étude sur la prolifération de la microalgue *Alexandrium minutum* en rade de Brest.

Chapelle, A., Le Gac, M., Labry, C., Siano, R., Quere, J., Caradec, F., Le Bec, E., Doner, A., Gouriou, J., 2015. The Bay of Brest (France), a new risky site for toxic *Alexandrium minutum* blooms and PSP shellfish contamination. Harmful algal news, 51, 4–5.

Chen, J., Ye, Q., Gu, H.-F., Li, H.-Y., Lv, S.-H., Liu, J.-S., Yang, W.-D., 2015. Variability in the allelopathic action of the *Alexandrium tamarense* species complex along the coast of China. Harmful Algae 47, 17–26. http://dx.doi.org/10.1016/j.hal.2015.05.008

Deeds, J., Place, A., 2006. Sterol-specific membrane interactions with the toxins from *Karlodinium micrum* (Dinophyceae) — a strategy for self-protection? African Journal of Marine Science 28, 421–425. https://doi.org/10.2989/18142320609504190

Dow, L., Stock, F., Peltekis, A., Szamosvári, D., Prothiwa, M., Lapointe, A., Böttcher, T., Bailleul, B., Vyverman, W., Kroth, P.G., Lepetit, B., 2020. The multifaceted inhibitory effects of an alkylquinolone on the diatom *Phaeodactylum tricornutum*. ChemBioChem 21, 1206–1216. https://doi.org/10.1002/cbic.201900612

Driscoll, W.W., Hackett, J.D., Ferrière, R., 2016. Eco-evolutionary feedbacks between private and public goods: evidence from toxic algal blooms. Ecology Letters 19, 81–97. https://doi.org/10.1111/ele.12533

Falciatore, A., Jaubert, M., Bouly, J.-P., Bailleul, B., Mock, T., 2020. Diatom molecular research comes of age: model species for studying phytoplankton biology and diversity. Plant Cell 32, 547–572. https://doi.org/10.1105/tpc.19.00158

Falkowski, P.G., Raven, J.A., 2007. Aquatic photosynthesis, 2nd ed. Princeton University Press, Princeton.

Fistarol, G., Legrand, C., Selander, E., Hummert, C., Stolte, W., Granéli, E., 2004. Allelopathy in *Alexandrium* spp.: effect on a natural plankton community and on algal monocultures. Aquatic Microbial Ecology. 35, 45–56. https://doi.org/10.3354/ame035045

706 Flores, H.S., Wikfors, G.H., Dam, H.G., 2012. Reactive oxygen species are linked to the
707 toxicity of the dinoflagellate *Alexandrium* spp. to protists. Aquatic Microbial Ecology 66, 199–
708 209. https://doi.org/10.3354/ame01570

709 Gantar, M., Berry, J.P., Thomas, S., Wang, M., Perez, R., Rein, K.S., 2008. Allelopathic activity
710 among Cyanobacteria and microalgae isolated from Florida freshwater habitats. FEMS
711 Microbiology Ecology 64, 55–64. https://doi.org/10.1111/j.1574-6941.2008.00439.x

712 Garces, E., 2004. Relationship between vegetative cells and cyst production during
713 *Alexandrium minutum* bloom in Arenys de Mar harbour (NW Mediterranean). Journal of
714 Plankton Research 26, 637–645. https://doi.org/10.1093/plankt/fbh065

715 Genty, B., Briantais, J.M., Baker, N.R., 1989. The relationship between the quantum yield of
716 photosynthetic electron transport and quenching of chlorophyll fluorescence. Biochimica et
717 Biophysica Acta - General Subjects 990, 87–92. https://doi.org/10.1016/S0304-
718 4165(89)80016-9

719 Granéli, E., Hansen, P.J., 2006. Allelopathy in harmful algae: a mechanism to compete for
720 resources?, in: Granéli, Edna, Turner, J.T. (Eds.), Ecology of Harmful Algae. Springer, Berlin
721 Heidelberg, pp. 189–201. https://doi.org/10.1007/978-3-540-32210-8_15

722 Guillard, R. R. L., & Hargraves, P. E. (1993). *Stichochrysis immobilis* is a diatom, not a
723 chrysophyte. Phycologia, 32, 234-236.

724 Hagmann, L., Jiittner, F., 1996. Fischerellin A, a Novel Photosystem-ll-inhibiting
725 allelochemical of the cyanobacterium *Fischerella muscicola* with antifungal and herbicidal
726 activity 37, 6539–6542.

727 Hakanen, P., Suikkanen, S., Kremp, A., 2014. Allelopathic activity of the toxic dinoflagellate
728 *Alexandrium ostenfeldii*: Intra-population variability and response of co-occurring
729 dinoflagellates. Harmful Algae 39, 287–294. https://doi.org/10.1016/j.hal.2014.08.005

730 Hattenrath-Lehmann, T.K., Gobler, C.J., 2011. Allelopathic inhibition of competing
731 phytoplankton by North American strains of the toxic dinoflagellate, *Alexandrium fundyense*:
732 Evidence from field experiments, laboratory experiments, and bloom events. Harmful Algae
733 11, 106–116. https://doi.org/10.1016/j.hal.2011.08.005

734 Heath, G.R., Harrison, P.L., Strong, P.N., Evans, S.D., Miller, K., 2018. Visualization of
735 diffusion limited antimicrobial peptide attack on supported lipid membranes. Soft Matter 14,
736 6146–6154. https://doi.org/10.1039/C8SM00707A

737 Hégaret, H., da Silva, P.M., Wikfors, G.H., Haberkorn, H., Shumway, S.E., Soudant, P., 2011.
738 In vitro interactions between several species of harmful algae and haemocytes of bivalve
739 molluscs. Cell Biol Toxicol 27, 249–266. https://doi.org/10.1007/s10565-011-9186-6

740 Jepras, R.I., Paul, F.E., Pearson, S.C., Wilkinson, M.J., Pharmaceuticals, S.B., Frontiers, N.,
741 Park, S., Cm, E., Kingdom, U., 1997. Rapid assessment of antibiotic effects on *Escherichia coli*
742 by flow cytometry. Antimicrobial agents and chemotherapy 41, 2001–2005.

743 John, U., Tillmann, U., Hülskötter, J., Alpermann, T.J., Wohlrab, S., Van de Waal, D.B., 2015.
744 Intraspecific facilitation by allelochemical mediated grazing protection within a toxigenic
745 dinoflagellate population. Proceedings of the Royal Society B : Biological Sciences 282,
746 20141268. https://doi.org/10.1098/rspb.2014.1268

747 Joliot, P., Delosme, R., 1974. Flash-induced 519 nm absorption change in green algae.
748 Biochimica et Biophysica Acta (BBA) - Bioenergetics 357, 267–284.
749 https://doi.org/10.1016/0005-2728(74)90066-8

750 Joliot, P., Joliot, A., 1979. Comparative study of the fluorescence yield and of the C550
751 absorption change at room temperature. Biochimica et Biophysica Acta (BBA) - Bioenergetics
752 546, 93–105. https://doi.org/10.1016/0005-2728(79)90173-7

753 Klughammer, C., Schreiber, U., 2008. Saturation pulse method for assessment of energy
754 conversion in PS I. PAM Application Notes 11–14.

755 Koppel, D.J., Gissi, F., Adams, M.S., King, C.K., Jolley, D.F., 2017. Chronic toxicity of five
756 metals to the polar marine microalga *Cryothecomonas armigera* – Application of a new
757 bioassay. Environmental Pollution 228, 211–221. https://doi.org/10.1016/j.envpol.2017.05.034

758 Legrand, C., Rengefors, K., Fistarol, G.O., Granéli, E., 2003. Allelopathy in phytoplankton -
759 biochemical, ecological and evolutionary aspects. Phycologia 42, 406–419.
760 https://doi.org/10.2216/i0031-8884-42-4-406.1

761 Lelong, A., Haberkorn, H., Le Goïc, N., Hégaret, H., Soudant, P., 2011a. A new insight into
762 allelopathic effects of *Alexandrium minutum* on photosynthesis and respiration of the diatom
763 *Chaetoceros neogracile* revealed by photosynthetic-performance analysis and flow cytometry.
764 Microbial Ecology 62, 919–930. https://doi.org/10.1007/s00248-011-9889-5

765 Lelong, A., Hégaret, H., Soudant, P., 2011. Cell-based measurements to assess physiological
766 status of *Pseudo-nitzschia multiseries*, a toxic diatom. Research in Microbiology 162, 969–981.
767 https://doi.org/10.1016/j.resmic.2011.06.005

Long, M., Tallec, K., Soudant, P., Lambert, C., Le Grand, F., Sarthou, G., Jolley, D., Hégaret, H., 2018a. A rapid quantitative fluorescence-based bioassay to study allelochemical interactions from *Alexandrium minutum*. Environmental Pollution 242, 1598-1605. https://doi.org/10.1016/j.envpol.2018.07.119

Long, M., Tallec, K., Soudant, P., Le Grand, F., Donval, A., Lambert, C., Sarthou, G., Jolley, D.F., Hégaret, H., 2018b. Allelochemicals from *Alexandrium minutum* induce rapid inhibition and modify the membranes from *Chaetoceros muelleri*. Algal Research 35, 508–518. https://doi.org/10.1016/j.algal.2018.09.023

Ma, H., Krock, B., Tillmann, U., Bickmeyer, U., Graeve, M., Cembella, A., 2011. Mode of action of membrane-disruptive lytic compounds from the marine dinoflagellate *Alexandrium tamarense*. Toxicon 58, 247–258. https://doi.org/10.1016/j.toxicon.2011.06.004

Ma, H., Krock, B., Tillmann, U., Cembella, A., 2009. Preliminary characterization of extracellular allelochemicals of the toxic marine dinoflagellate *Alexandrium tamarense* using a *Rhodomonas salina* bioassay. Marine Drugs 7, 497–522. https://doi.org/10.3390/md7040497

Marie, D., Brussaard, C.P.D., Thyrhaug, R., Bratbak, G., Vaulot, D., 1999. Enumeration of marine viruses in culture and natural samples by flow cytometry. Applied and Environmental Microbiology 65, 45–52.

Meng, F. Q., Song, J. T., Zhou, J., & Cai, Z. H. (2019). Transcriptomic profile and sexual reproduction-relevant genes of *Alexandrium minutum* in response to nutritional deficiency. Frontiers in Microbiology, 10, 2629.

Morel, F.M.M., Rueter, J.G., Anderson, D.M., Guillard, R.R.L., 1979. Aquil: a chemically defined phytoplankton culture medium for trace metal studies. Journal of Phycology, 15, 135-141. https://doi.org/10.1111/j.1529-8817.1979.tb02976.x

Morsy, N., Houdai, T., Konoki, K., Matsumori, N., Oishi, T., Murata, M., 2008a. Effects of lipid constituents on membrane-permeabilizing activity of amphidinols. Bioorganic & Medicinal Chemistry 16, 3084–3090. https://doi.org/10.1016/j.bmc.2007.12.029

Morsy, N., Konoki, K., Houdai, T., Matsumori, N., Oishi, T., Murata, M., Aimoto, S., 2008b. Roles of integral protein in membrane permeabilization by amphidinols. Biochimica et Biophysica Acta (BBA) - Biomembranes 1778, 1453–1459. https://doi.org/10.1016/j.bbamem.2008.01.018

Naghdi, F.G., Bai, X., Thomas-Hall, S.R., Sharma, K., Schenk, P.M., 2016. Lipid extraction from wet *Chaetoceros muelleri* culture and evaluation of remaining defatted biomass. Algal Research 20, 205–212. https://doi.org/10.1016/j.algal.2016.10.011

Paul, C., Barofsky, A., Vidoudez, C., Pohnert, G., 2009. Diatom exudates influence metabolism and cell growth of co-cultured diatom species. Marine Ecology Progress Series 389, 61–70. https://doi.org/10.3354/meps08162

Place, A.R., Bowers, H.A., Bachvaroff, T.R., Adolf, J.E., Deeds, J.R., Sheng, J., 2012. *Karlodinium veneficum*—The little dinoflagellate with a big bite. Harmful Algae 14, 179–195. https://doi.org/10.1016/j.hal.2011.10.02

Poulin, R.X., Hogan, S., Poulson-ellestad, K.L., Brown, E., 2018. *Karenia brevis* allelopathy compromises the lipidome, membrane integrity, and photosynthesis of competitors. Scientific Reports 8, 1–9. https://doi.org/10.1038/s41598-018-27845-9

Prado, R., Rioboo, C., Herrero, C., Cid, A., 2012. Screening acute cytotoxicity biomarkers using a microalga as test organism. Ecotoxicology and Environmental Safety 86, 219–226. https://doi.org/10.1016/j.ecoenv.2012.09.015

Prince, E.K., Myers, T.L., Kubanek, J., 2008. Effects of harmful algal blooms on competitors: Allelopathic mechanisms of the red tide dinoflagellate *Karenia brevis*. Limnology and Oceanography 53, 531–541. https://doi.org/10.4319/lo.2008.53.2.0531

Pushparaj, B., Pelosi, E., Jüttner, F., 1998. Toxicological analysis of the marine cyanobacterium *Nodularia harveyana*. Journal of Applied Phycology 10, 527–530. https://doi.org/10.1023/A:1008080615337

Rappaport, F., Béal, D., Joliot, A., Joliot, P., 2007. On the advantages of using green light to study fluorescence yield changes in leaves. Biochimica et Biophysica Acta (BBA) - Bioenergetics 1767, 56–65. https://doi.org/10.1016/j.bbabio.2006.10.002

Satake, M., Honma, D., Watanabe, R., Oshima, Y., 2019. Alexandrolide, a diatom growth inhibitor isolated from the dinoflagellate *Alexandrium catenella*. Tetrahedron Letters 60, 1341–1344. https://doi.org/10.1016/j.tetlet.2019.04.019

Seoane, M., Esperanza, M., Rioboo, C., Herrero, C., Cid, Á., 2017. Flow cytometric assay to assess short-term effects of personal care products on the marine microalga *Tetraselmis suecica*. Chemosphere 171, 339–347. https://doi.org/10.1016/j.chemosphere.2016.12.097

828 Shikanai, T., 2007. Cyclic Electron Transport Around Photosystem I: Genetic Approaches.
829 Annual Review of Plant Biology 58, 199–217.
830 https://doi.org/10.1146/annurev.arplant.58.091406.110525

831 Suikkanen, S., Hakanen, P., Spilling, K., Kremp, A., 2011. Allelopathic effects of Baltic Sea
832 spring bloom dinoflagellates on co-occurring phytoplankton. Marine Ecology Progress Series
833 439, 45–55. https://doi.org/10.3354/meps09356

834 Ternon, E., Pavaux, A.S., Marro, S., Thomas, O.P., Lemée, R., 2018. Allelopathic interactions
835 between the benthic toxic dinoflagellate *Ostreopsis* cf. *ovata* and a co-occurring diatom.
836 Harmful Algae 75, 35–44. https://doi.org/10.1016/j.hal.2018.04.003

837 Tillmann, U., 2003. Kill and eat your predator: a winning strategy of the planktonic flagellate
838 *Prymnesium parvum*. Aquatic Microbial Ecology. 32, 73–84.
839 https://doi.org/10.3354/ame032073

840 Tillmann, U., John, U., 2002. Toxic effects of *Alexandrium* spp. on heterotrophic
841 dinoflagellates: an allelochemical defence mechanism independent of PSP-toxin content.
842 Marine ecology progress series. 230, 47–58. https://doi.org/10.3354/meps230047

843 Tillmann, U., John, U., Cembella, A., 2007a. On the allelochemical potency of the marine
844 dinoflagellate *Alexandrium ostenfeldii* against heterotrophic and autotrophic protists. Journal
845 of Plankton Research 29, 527–543. https://doi.org/10.1093/plankt/fbm034

846 Wang, R., Wang, J., Xue, Q., Sha, X., Tan, L., Guo, X., 2017. Allelopathic interactions between
847 *Skeletonema costatum* and *Alexandrium minutum*. Chemistry and Ecology 33, 485–498.
848 https://doi.org/10.1080/02757540.2017.1332187

849 Waters, A.L., Oh, J., Place, A.R., Hamann, M.T., 2015. Stereochemical studies of the karlotoxin
850 class using NMR spectroscopy and DP4 chemical-shift analysis: insights into their mechanism
851 of action. Angewandte Chemie. 127, 15931–15936. https://doi.org/10.1002/ange.201507418

852 Witt, H.T., 1979. Energy conversion in the functionnal membrane of photosynthesis. Analysis
853 by light pulse and electric pulse methods. Biochimica et Biophysica Acta 505, 355–427.

854 Xu, N., Tang, Y., Qin, J., Duan, S., Gobler, C., 2015. Ability of the marine diatoms *Pseudo-*
855 *nitzschia* multiseries and *P. pungens* to inhibit the growth of co-occurring phytoplankton via
856 allelopathy. Aquatic Microbial Ecology. 74, 29–41. https://doi.org/10.3354/ame01724

857

Figures

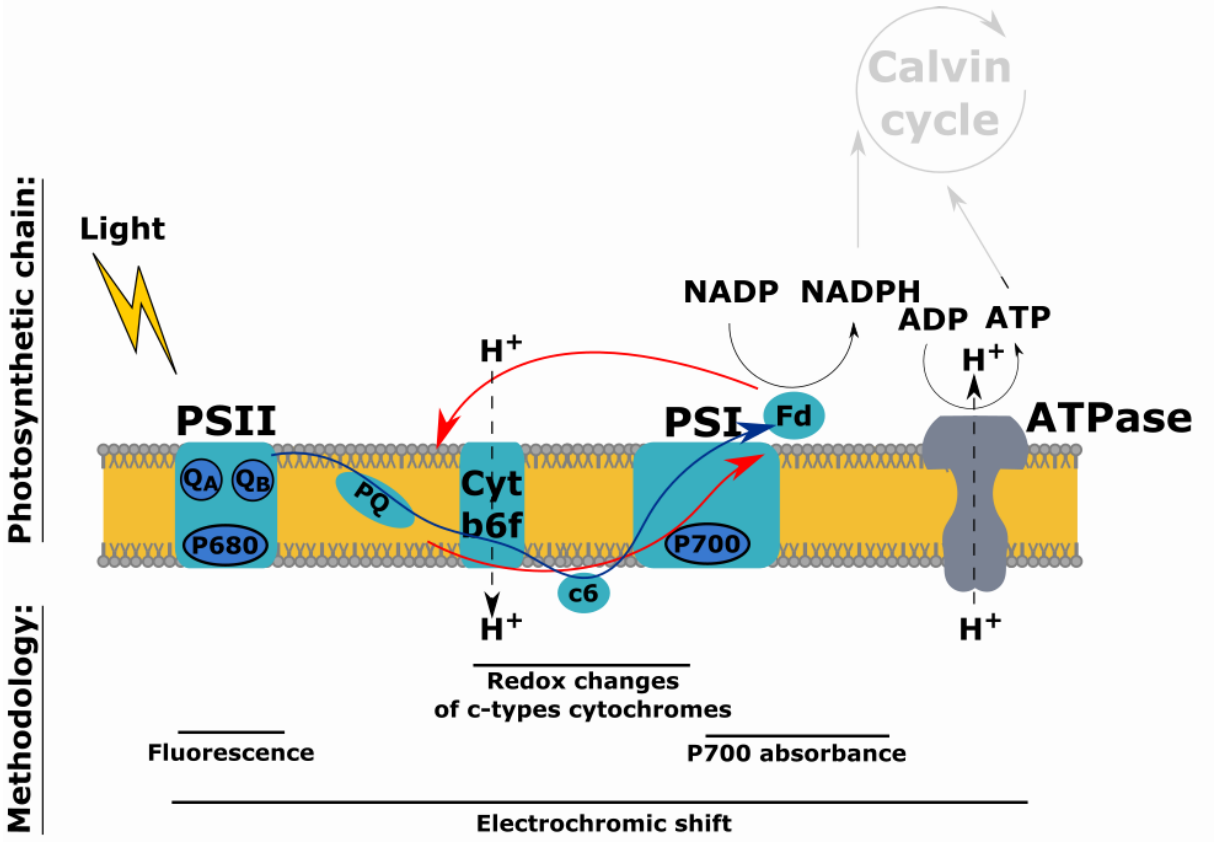

Figure 1: Schematic figure of the photosynthetic chain and methodology used for measuring the different photosynthetic components. The blue arrow represents the linear electron flow; the red arrows represent the cyclic electron flow around the PSI. PSI and PSII: Photosystems I and II, Q_A and Q_B: Quinones A and B, PQ : Plastoquinone, Cyt b6f : Cytochrome b6f, c6 : Cytochrome 6, P700: PSI reaction center, Fd: Ferredoxin

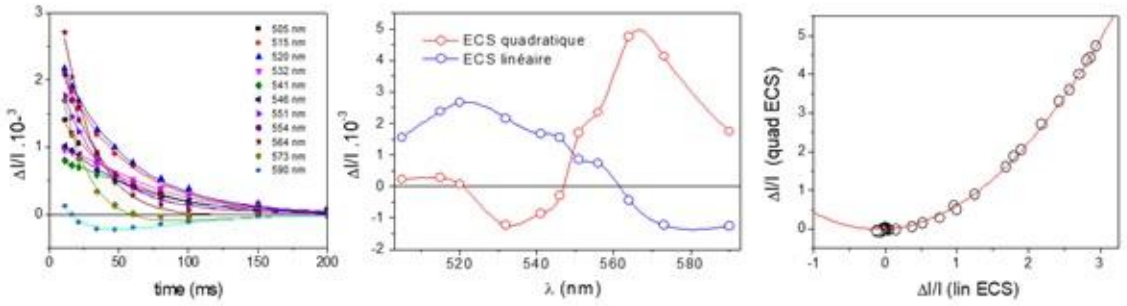

Figure 2: Deconvolution of the linear and quadratic ECS contributions in Chaetoceros muelleri, *treated with 100µM CCCP (see Methods). Panel A: Relaxation of the absorption changes (ΔI/I) induced by a saturating pulse of light, at different wavelengths. Lines are extrapolation of the experimental points by a sum of two exponentials (see Methods). Panel B: the linear and quadratic ECS spectra are obtained from the amplitudes of the two exponentials in the extrapolation shown in the left panel (see Methods). Panel C: Absorption changes at 564 nm (where only quadratic ECS contributes, see panel B) is plotted as a function of the absorption change at 520 nm*

(where only linear ECS contributes, see panel B). The experimental points are fitted by a quadratic function (red line), which validates the deconvolution procedure.

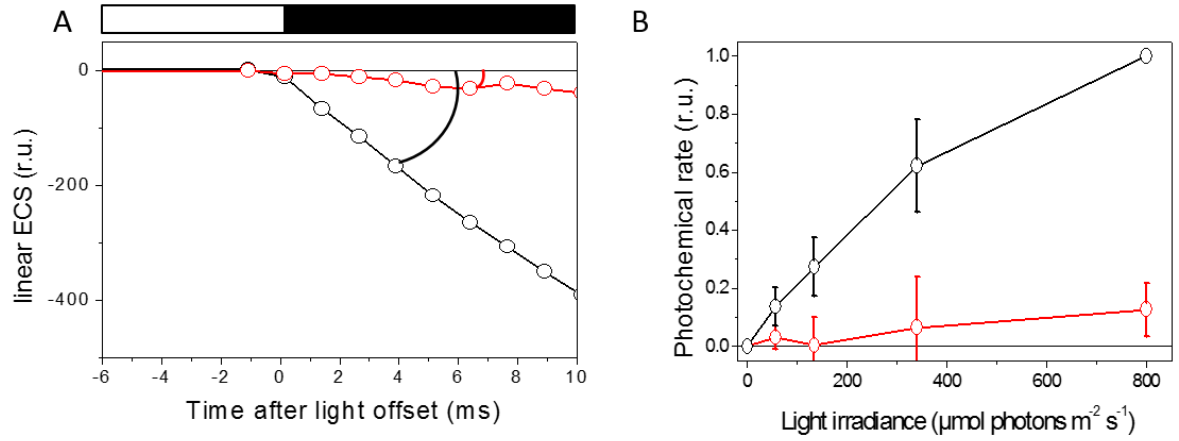

Figure 3: Effect of A. minutum *supernatant on the overall photosynthesis activity. A) Linear ECS changes after turning off the light in the absence (black dots/lines) and presence (red dots/lines) of* A. minutum *filtrate. White bar represents the light phase (here, 800 µmol photons m^{-2} s^{-1}), dark bar the period of darkness. The arc of circles represents the change of slope at the light offset. B. Light dependency of photochemical rates of* C. muelleri *with (red dots/lines) or without (black dots/lines)* A. minutum *filtrate. Data were normalized to the maximal value at 800 µmol photons m^{-2} s^{-1} in the untreated sample (see Methods). Results are expressed in relative unit (r.u.). Error bars represent standard deviation (n = 4).*

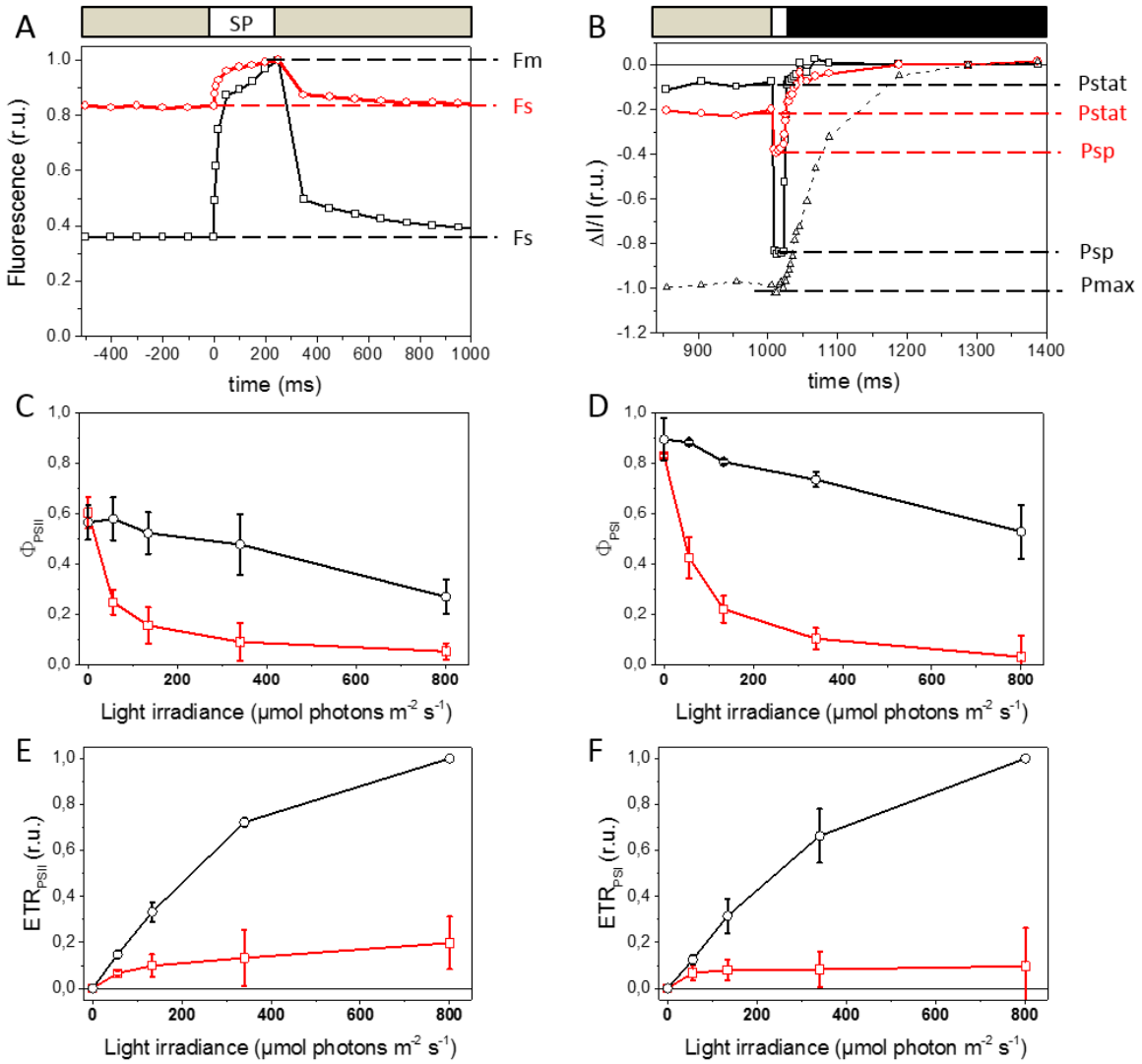

881

882 *Figure 4: Effects of* A. minutum *filtrate on the activity of PSII (A, C, E) and PSI (B, D, F) of* C. muelleri. *Dark:*
883 *control, red: in the presence of* A. minutum *filtrate. A/B: The fluorescence and P700 measurements for the*
884 *calculation of PSII (A) and PSI (B) quantum yields (see Methods for explanations of the different parameters). In*
885 *panel B, the dashed lines and rectangles show the absorption changes in the control with DCMU. Grey bars above*
886 *the panels represent the light phase (here, 340 µmol photons* m^{-2} s^{-1}*), dark bar is the period of darkness and white*
887 *"SP" phase shows the saturating pulse phase. Data in panels A and B were obtained under 340 µmol photons* m^{-2} s^{-1}
888 *actinic light. C/D: Light dependencies of the quantum yields of PSII (C) and PSI (D). E/F: Light dependency*
889 *of the electron transfer rates through PSII (*ETR_{PSII}*, E) and through PSI (*ETR_{PSI}*, F). Results are normalized to the*
890 *value at the highest intensity (see Methods). Error bars represent standard deviation (n = 3 for the right panels*
891 *(B, D, F), n=6 for the left panels (A, C, E)).*

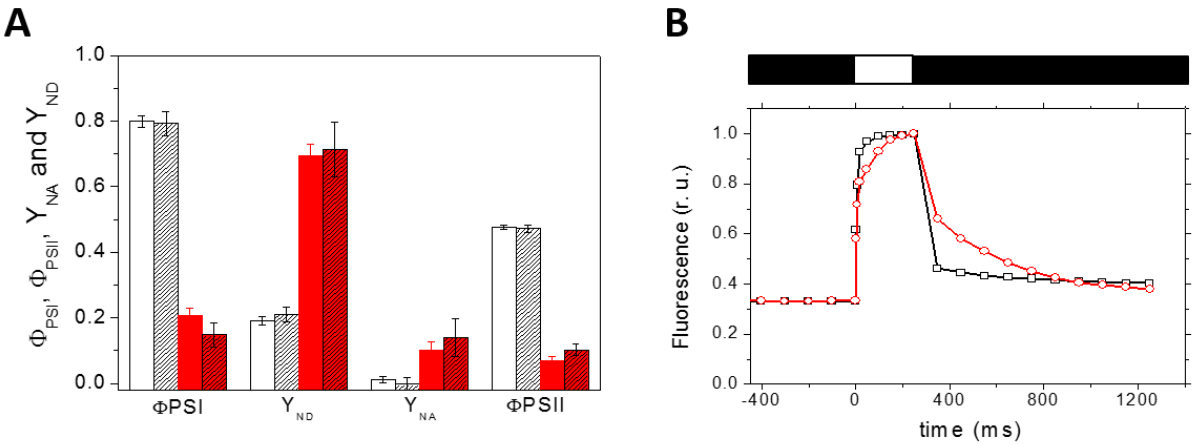

Figure 5 Short-term effect of A. minutum *supernatant on the PSI and PSII activities of* C. muelleri. *A: The quantum yields of PSII and PSI, as well as the donor-side (Y(ND)) and acceptor-side (Y(NA)) limitations are shown for the control (white bars) and in the presence of A. minutum filtrate (red bars), with (hatched) and without (plain) the PSI acceptor methylviologen (1mM). All experiments were performed at 340 µmol photons* m^{-2} s^{-1} *actinic light. Error bars represent standard deviation (n = 3). B:* F_v/F_m *for the control (black dots/lines) and filtrate (red dots/lines) exposed samples were 0.66 ± 0.02 and 0.69 ± 0.03, respectively. A saturating pulse (white rectangle) is applied on dark-adapted (black rectangle) samples to measure* F_v/F_m. *Results are normalized to the Fm.*

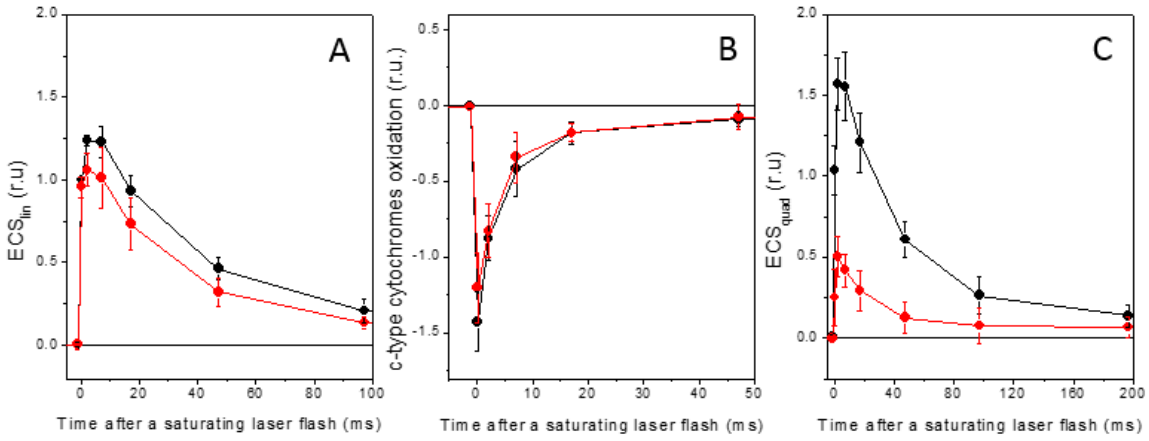

Figure 6. Kinetic of the linear ECS.(A), c-type cytochromes oxidation (B) and quadratic ECS (C) after a saturating laser flash. Dark: control diatom cells. Red: After 10 min of incubation with the filtrate of A. minutum. *The linear and quadratic ECS and c-type cytochrome are calculated from absorption changes at 520, 554, 564 nm (see Methods). Error bars represent standard deviation (n = 4).*

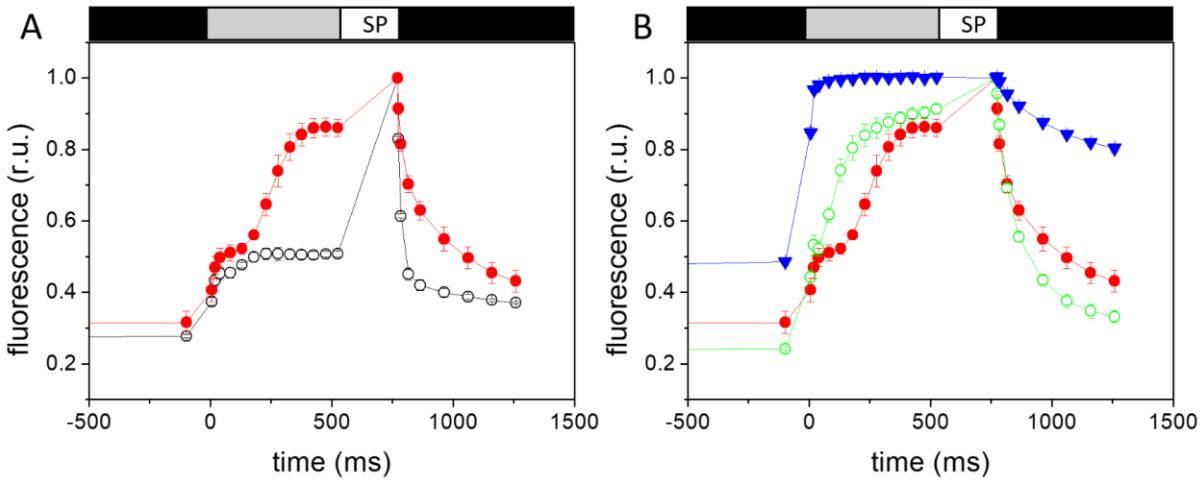

905

906 *Figure 7. Effect of* A. minutum *filtrate on* C. muelleri *fluorescence induction and relaxation curves. A:*
907 *Fluorescence induction curve of* C. muelleri *control (black dots/lines) and in presence of* A. minutum *filtrate (red*
908 *dots/lines). B: Fluorescence induction curve of* C. muelleri *in the presence of* A. minutum *filtrate (red dots/lines),*
909 *with DCMU (10µM) (blue dots/lines) and DBMIB (0.5 µM) (green dots/lines). Error bars correspond to the S.D*
910 *(3 independent replicates). White and black bars above the panels represent the light and dark periods,*
911 *respectively.*

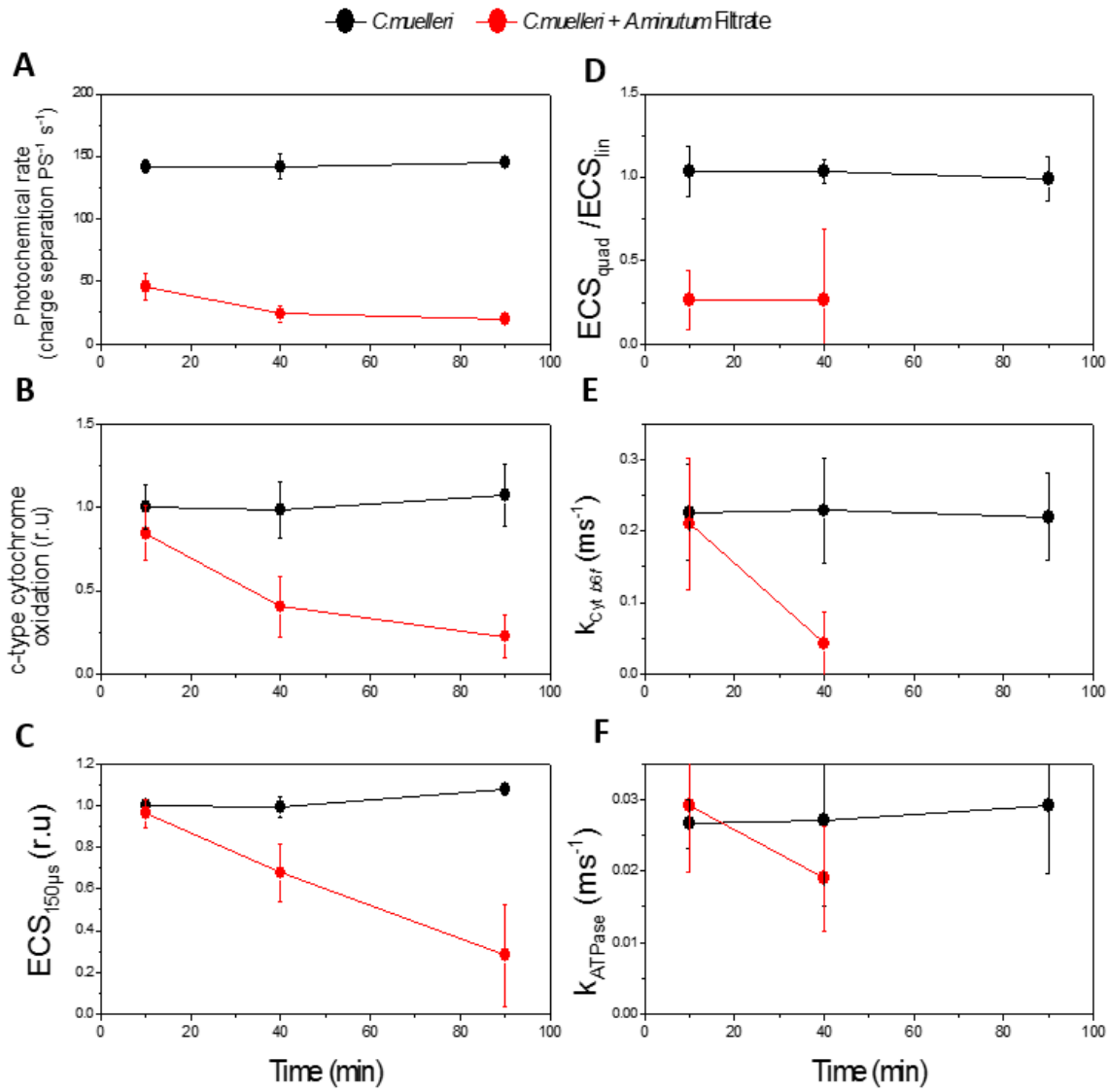

912

913 *Figure 8. Effect of the filtrate of* A. minutum *on photosynthetic complexes and overall photosynthesis at different*
914 *times of exposure (10, 40 and 90 minutes). Black: control. Red: cells treated with the filtrate of* A. minutum. *A:*
915 *photochemical rate measured after 3 minutes illumination at 800 µmol photons* m^{-2} s^{-1}. *B: ratio of the quadratic-*
916 *to-linear ECS increase 160 µs after the saturating laser flash. C/D: Extent of oxidation (C) and rate of re-reduction*
917 *(D) of c-type cytochromes. E/F: fast rise (a phase, 160 µs after the saturating laser flash, E) and rate of decay of*
918 *linear ECS (F). The linear and quadratic ECS and c-type cytochrome oxidation are calculated from absorption*
919 *changes at 520, 554, 564 nm (see Methods). The ECS and c-type cytochromes signals become too small after 90*
920 *minutes exposure to allow measurements of the quadratic-to-linear ECS, or* b_6f *and ATPase rate constants. Error*
921 *bars represent standard deviation (n = 3-5).*

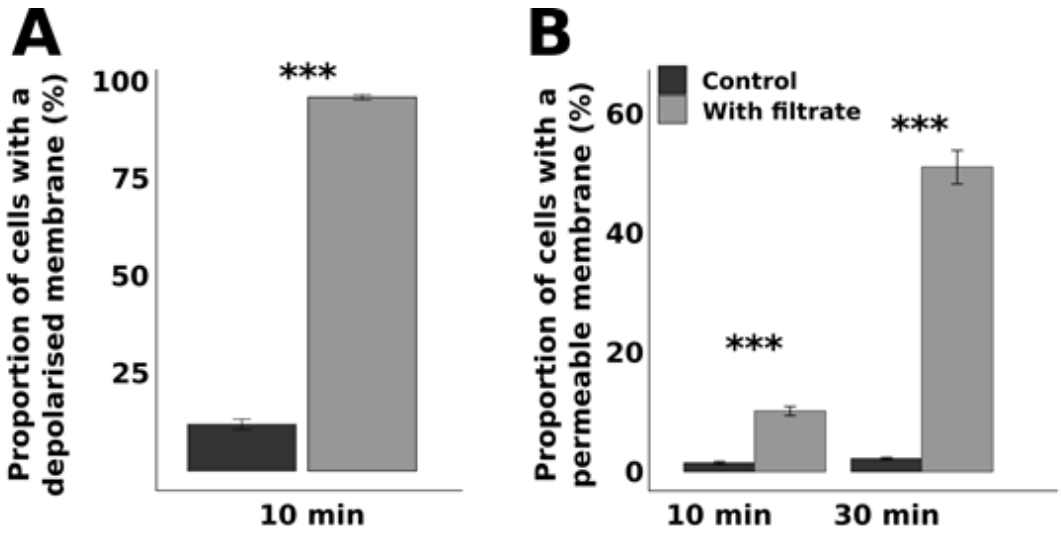

Figure 9: Effect of A. minutum *filtrate on* C. muelleri *cytoplasmic membranes. A) Variation in the proportion of cells with a depolarized membrane after 10 min of exposure to the filtrate (labelled with DiBAC$_4$(3)). B) Variation in the proportion of cells with a permeable membrane after 10 and 30 min of exposure to the filtrate (labelled with SytoxGreen). Cells in the control are shown in dark grey and cells in the presence of A. minutum filtrate are shown in light grey. *** indicate a level of significance < 0.001. Results are expressed as the mean ± standard error (n = 3).*

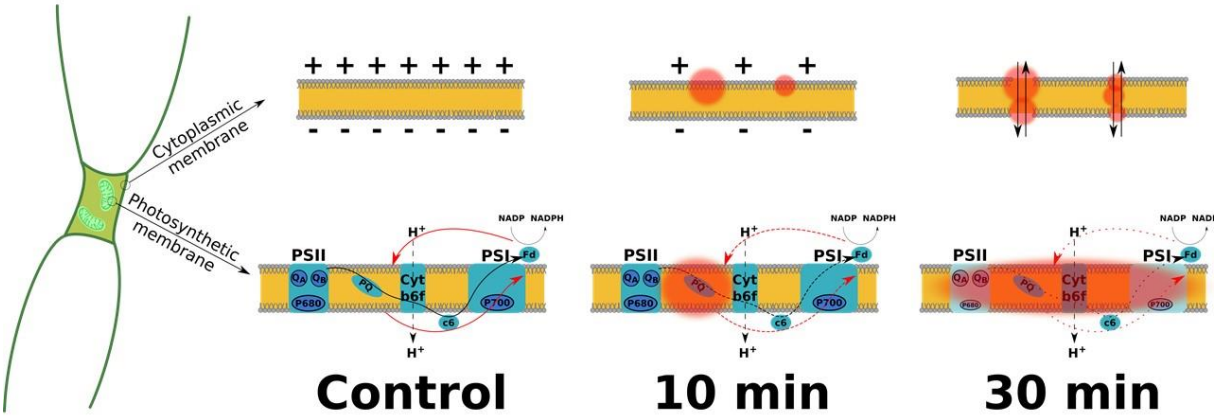

Figure 10: Schematic figure of the cascade of events occurring to the cytoplasmic (top) and photosynthetic membranes (bottom) following the exposure to A. minutum filtrate. The red circles represent the membrane components affected by allelochemicals. The blue arrow represents the linear electron flow and the red arrows represent the cyclic electron flow around PSI. PSI and PSII: Photosystems I and II, Q_A and Q_B: Quinones A and B, PQ : Plastoquinone, Cyt b6f : Cytochrome b6f, c6 : Cytochrome 6, P700: PSI reaction center, Fd: Ferredoxin.

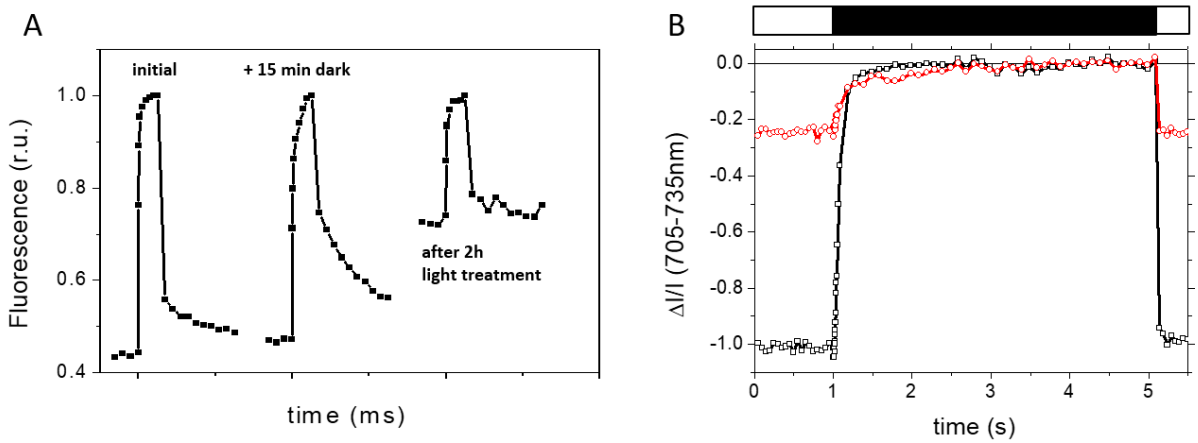

937

938 **Fig. S1** Effect of *Alexandrium*'s allelochemicals on fluorescence induction and relaxation curves

939 *(A) Fluorescence of C. muelleri exposed to A. minutum filtrate where a saturating pulse is applied immediately*
940 *after exposure, after 15 min of dark exposure and after 2 hours of light treatments. (B) Relative amount of P700*
941 *photo-oxidizable in absence (black dots/lines) and presence (red dots/lines) of A. minutum filtrate given by the*
942 *change in ΔI/I under different light conditions. Results are expressed in relative unit (r.u.).*

943

944